Electronic density of states in amorphous selenium

2004 J. Phys.: Condens. Matter 16 S5253

(http://iopscience.iop.org/0953-8984/16/44/022)

INSTITUTE OF PHYSICS PUBLISHING JOURNAL OF PHYSICS: CONDENSED MATTER

J. Phys.: Condens. Matter **16** (2004) S5253–S5264 PII: S0953-8984(04)84989-0

Electronic density of states in amorphous selenium

M L Benkhedir, M Brinza and G J Adriaenssens

Laboratorium voor Halfgeleiderfysica, University of Leuven, Celestijnenlaan 200D, B-3001 Leuven, Belgium

Received 14 August 2004
Published 22 October 2004
Online at stacks.iop.org/JPhysCM/16/S5253
doi:10.1088/0953-8984/16/44/022

Abstract

Steady-state and transient photoconductivity methods are used to investigate the electronic density of states in evaporated layers of amorphous selenium. From the temperature dependence of the steady-state photocurrent and, independently, from an analysis of the post-transit currents of time-of-flight transients, energy levels in the gap at 1.43 ± 0.02 eV and 0.40 ± 0.02 eV above the valence band have been determined for the occupied state of the negative-U centres. An absorption band around 1.50 eV is seen in the spectral distribution of the photocurrent. The distribution of tail states may—to first approximation—be described by a steep exponential with a characteristic width of ∼24 meV at the valence band and a more steeply declining functional of similar width at the conduction band.

1. Introduction

Discussions of the electronic density of states (DOS) in the band gap of the chalcogenide semiconductors have traditionally focused on the prominent distributions of tail states that result from the lattice disorder and on the coordination defects that produce localized states deeper in the gap [1]. In particular the latter have received much attention because they exhibit a negative effective electron correlation energy, making doubly occupied defect centres energetically more favourable than the singly occupied ones. These so-called negative-U centres were introduced in the electronic structure models of the chalcogenides [2, 3] to account for the fact that no electron spin resonance signals were observed in amorphous selenium (a-Se) and a host of other chalcogenides [4], contrary to the expectation that dangling bonds in the amorphous lattice would produce such signals. They have become one of the hallmarks of the chalcogenide glasses, even though some disagreement persists on the need to invoke their presence [5].

From the experimental side, the different aspects of the DOS have been examined most comprehensively for the arsenic chalcogenides, with less attention being paid to a-Se and other members of the chalcogenide group. From the beginning, available results from dark and photoconductivity studies and from optical and photoluminescence spectroscopy

of amorphous As_2Se_3 and As_2Te_3 samples allowed verification of the implications of the negative-U model [6, 7]. The basis of the model is the ability of the chalcogenide lattice to undergo polaronic deformation to the extent that the configurational energy gain at double occupancy of a defect site outweighs the electron–electron repulsion energy. As the polaronic energy shift depends on the charge state of the defect centre, transitions involving occupied centres reflect different energy positions than transitions to unoccupied centres. In addition, optical transitions to and from the defect centres will occur at different energies from thermally induced ones since, unlike the photons of the former, the phonons of the latter carry the necessary momentum to cover the configurational changes. These facts result in a multi-level energy diagram for the negative-U defects, with negatively and positively charged sites forming the equilibrium configuration of the system [3]. The different transitions involved in optical absorption [8] and photoconductive [9] or radiative [10, 11] recombination thus confirmed the energy scheme proposed for the model in the original papers [12]. Defect densities of the order of 10^{17}–10^{18} cm^{-3} were suggested [6, 12].

The tail-state distribution of the chalcogenides has been studied and discussed primarily for As_2Se_3 samples. Transient photocurrent measurements reveal power-law current decays of the type $I_{ph} \propto t^{-(1-\alpha)}$ after pulsed excitation of the As_2Se_3, with the exponent being temperature dependent according to $\alpha \cong T/T_0$. When interpreted in the framework of the multiple-trapping (MT) transport model [13], these results agree very well with an exponential distribution of states $g(E) = g(0)\exp(-E/E_0)$ with $E_0 = kT_0 \cong 50$ meV [14]. The exponential DOS was even found to extend up to 0.86 eV above the valence band edge [15]. It was pointed out in [15] that this last result raises questions concerning the relationship between those tail states and the gap states introduced by the coordination defects. No evidence for the latter was observed in the transient photoconductivity experiments. Subsequent studies have shown that enhanced, non-equilibrium concentrations of the defect states may actually be observed through transient photoconductivity [16], and that the different nature of tail and gap states can lead to different sensitivity to them between steady-state and transient measurements [1].

Compared to the case of the arsenic chalcogenides, and especially when compared to As_2Se_3, relatively little information has become available on the electronic density of states in the a-Se band gap. Until some recent attempts [17, 18] to extract DOS information from time-of-flight (TOF) transient photoconductivity measurements, only a few scarce transient photocurrent [19] and xerographic discharge [20] results were interpreted in terms of DOS features. This fact contrasts strongly with the prominent use of a-Se as a model system for the negative-U centres. Indeed, the singly coordinated, negatively charged C_1^- site and the threefold coordinated, positively charged C_3^+ that were identified as the most likely negative-U configurations in a-Se [21], have become the prototypal examples in literature discussions of the negative-U model [22, 23]. A recent paper has attempted to fill in a few of the gaps in our knowledge of the a-Se DOS [24], but the overall picture remains vague and uncertainties on resolved defect levels remain large. Contributing to this lack of precise information are undoubtedly the facts that a-Se is a very resistive material with a room-temperature band gap of nearly 2 eV, which makes it difficult to maintain good precision with electrical measurements below room temperature, and that the glass temperature of a-Se is only 40 °C, which limits the measurement range above room temperature.

In the present contribution, we will apply a combination of steady-state and transient photoconductivity techniques to several series of thermally evaporated a-Se films to bring our knowledge of the DOS in a-Se to a level that is comparable to the one of the arsenic chalcogenides. The general picture that emerges confirms a-Se as a typical element of the group of negative-U chalcogenide glasses, erasing earlier doubts [25] that may have existed on this point.

2. Experimental details

a-Se films with thickness varying from 1 to 20 μm were evaporated in a vacuum background of 10^{-2} Pa from 99.995% pure Se (Alfa Aesar) onto high-resistivity Corning 7059 glass substrates. For electrical measurements, either gap-cell or sandwich-cell configurations were used. Gap cells had evaporated gold electrodes on top of the films with active areas of 0.5 mm $\times$ 10 mm. Aluminium electrodes were used for the sandwich cells, one pre-deposited on the glass substrate and the top ones being semi-transparent circular dots of 2 or 4 mm diameter. The substrate temperature was not regulated during the evaporations, but x-ray examination of several films proved that they were fully amorphous. A further set of samples deposited on either glass or aluminium substrates and with Au and Pt top contacts was provided by Professor Kasap (University of Saskatchewan). Their thickness ranged from 8 to 300 μm.

DC conductivity measurements were carried out in a 5×10^{-3} Pa atmosphere by means of a Keithley 428 current amplifier and a Agilent 3440a millivoltmeter, with typically 100 V applied across a gap cell and 5 V for a sandwich cell. For measuring the steady-state photoconductivity (SSPC), a 15 mW He–Ne laser (632.8 nm) or an infra-red light emitting diode (LED, 890 nm, 1.7 mW cm^{-2} at 50 mA) were used as monochromatic light sources. Spectral response curves were obtained with a 250 W tungsten–halogen lamp plus grating monochromator (10 nm bandpass). Calibrated neutral density filters served to modify the light intensity.

Transient photocurrent measurements were carried out with a standard time-of-flight (TOF) set-up. The 337 nm light pulse of a pulsed LSI nitrogen laser triggered a dye cell with Coumarin 440 to produce a $\sim$6 ns long, 440 nm pulse. Measurements were performed using single light pulses, i.e. without signal averaging. The signal, displayed on an IWATSU 8132 digitizing storage oscilloscope, was transferred into and processed by a computer. An HP 214B pulse generator was used for the bias voltage for times up to 10 ms, and a dc voltage supply was used for longer times.

For both TOF and SSPC measurements, the sample was placed on a metal support in the vacuum chamber. The sample temperature was controlled to better than 1 K by a combination of liquid nitrogen cooling and regulated electrical heating of the sample support.

3. Photoconductivity results and analysis

3.1. Steady-state measurements

Figure 1 shows the temperature dependence of the steady-state photocurrent in a 265 μm thick a-Se sandwich cell, when illuminated at 890 nm with the LED, as well as the dark current through the cell. The change-over from rising currents with rising inverse temperature at the high-temperature end to decreasing currents at the low-temperature end corresponds to the traditional pattern observed in numerous chalcogenide glasses [9, 16, 26, 27]. At the higher temperatures, i.e. at high concentrations of thermally generated carriers, monomolecular recombination controls the magnitude of the photocurrent [9, 26] and the activation energy, ΔE_{m}, of the photocurrent in that range indicates the position above the material's Fermi level of a donor-like recombination centre. On the low-temperature side, the optically generated carriers dominate the conductivity, the recombination is mostly bimolecular, and the photocurrent activation energy in this region, ΔE_{b}, can be linked to an acceptor-like recombination centre located $2\Delta E_{\mathrm{b}}$ above the valence band mobility edge [9]. From figure 1, $\Delta E_{\mathrm{m}} = 0.50 \pm 0.02$ eV can be determined with good precision, but the temperature range available below the photocurrent maximum is too limited to permit the determination of ΔE_{b} with similar precision. Consequently, the value $\Delta E_{\mathrm{b}} = 0.18 \pm 0.03$ eV reported in [24] on the basis of measurements over a wider temperature range—be it on thinner samples—will be used in later discussions.

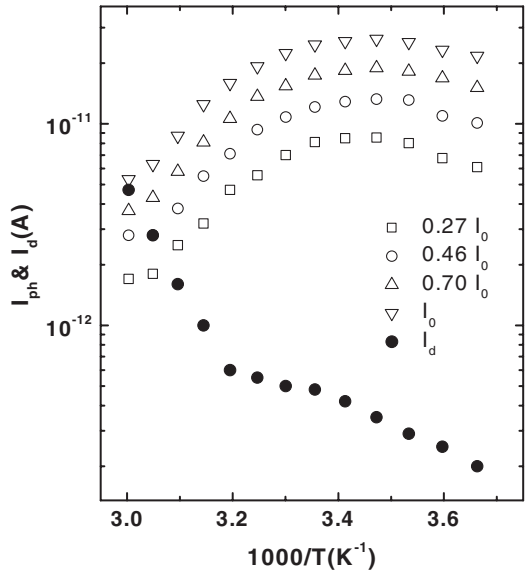

Figure 1. Temperature dependence of the steady-state photocurrent for four intensities of 890 nm illumination, with 100 V applied across a 265 μm thick a-Se sandwich cell. The reference light intensity is $I_0 = 4 \times 10^{16}$ photons cm^{-2} s^{-1}. The full symbols indicate the level of the underlying dark current.

The dark conductivity data shown in figure 1 testify to the presence of two different conduction mechanisms in the sample. For $10^3/T < 3.2$ K^{-1}, an activation energy of $\sim$0.92 eV is observed, in general agreement with results from other samples and with reported literature values in the 0.9–1.0 eV range. To first approximation this energy reflects the distance E_F–E_V between the valence band mobility edge and the Fermi level (holes being the mobile carriers in the chalcogenides), and indicates that band transport dominates. At lower temperatures a hopping current component is dominant with the approximate activation energy of 0.25 eV reflecting injection across the aluminium oxide barrier at the bottom contact of the sample. Depending on the individual sample, the magnitude of this injected current can vary widely, but the activation energy remains the same.

The recombination centres, discussed above and located at $E_V + 2\Delta E_b$ and $E_F + \Delta E_m$, have been identified in the literature as the thermally accessible levels of the negative-U energy diagram [6, 7, 28]. Further information on some of the optical transitions in the diagram may also be deduced from photocurrent measurements. Steady-state photoconductivity, of course, reflects the equilibrium between optical excitation and thermal recombination of charge carriers. The spectral distribution of the photocurrent, displayed in figure 2, therefore logically reflects the increasing absorption in the increasing tail-state density as the excitation energy approaches the optical absorption edge of $\sim$2 eV, but it also shows a shoulder in the 1.45–1.5 eV region that can be linked to additional absorption between the bands and the defect centres. Specifically, that energy could correspond to transitions between the valence band and the D^+ centre, or between the D^- centre and the conduction band.

3.2. Transient measurements

Transient photocurrent techniques have been used in chalcogenide research mainly to test the tail-state distribution in the arsenic compounds, or to measure the carrier mobility in a-As_2Se_3

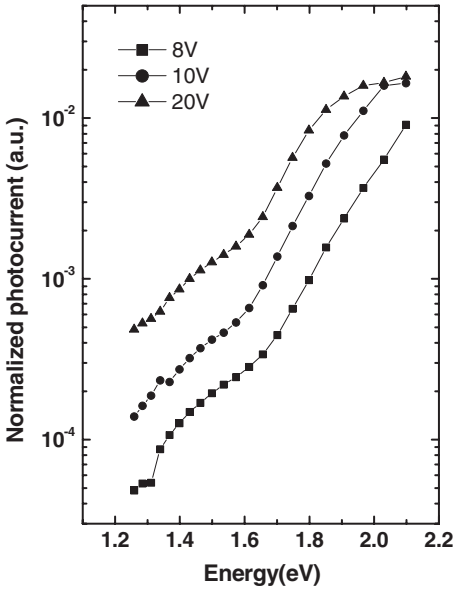

Figure 2. Spectral distribution of the steady-state photocurrent in a-Se, normalized to a constant number of 4×10^{12} photons $\mathrm{cm}^{-2}\ \mathrm{s}^{-1}$.

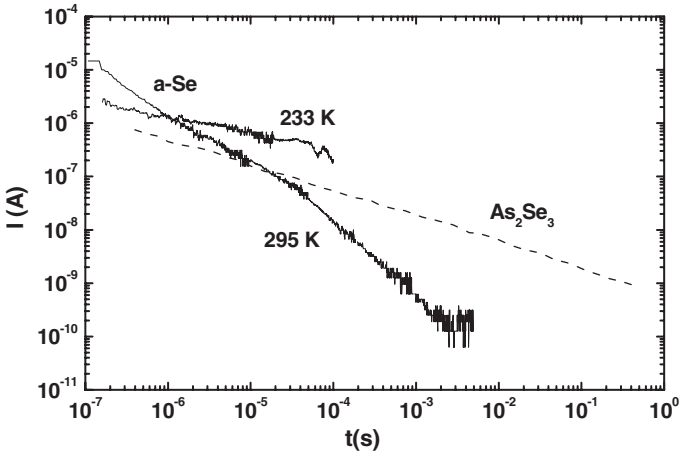

Figure 3. Time evolution of the transient photocurrent in a-Se gap cells after pulsed excitation at 440 nm. Part of the a-As_2Se_3 transient from [15] is shown for comparison.

and a-Se, but through the post-transit analysis of time-of-flight signals, they can also provide information on the location of defect levels in the gap. We have made use of all of those possibilities. In figure 3, the transient current decay after pulsed optical excitation from a-Se samples is compared to the well-known room-temperature a-As_2Se_3 decay from [15]. At first sight, a power-law current decay $I_{\mathrm{ph}} \propto t^{-(1-\alpha)}$ of the type seen for a-As_2Se_3 seems to be observed for the a-Se samples as well. However, the parameter α would then have the inverse temperature dependence for a-Se from the T/T_0 that would signal an exponential DOS. Using the slope measured at the lowest temperature of 233 K and $\alpha = T/T_0$, a value $T_0 \approx 320$ K

($E_0 \approx 28$ meV) follows. This T_0 value conceivably indicates that at higher measurement temperatures α lies too close to the value 1 for the standard MT analysis of carrier transport in an exponential DOS to remain valid.

This standard MT analysis, which has successfully been used in earlier studies of a-As_2Se_3 [14, 15], also predicts that the width E_0 of the exponential tail can be deduced from the field dependence of the carrier drift mobility, as measured in a TOF experiment, according to the relationship

$$\mu_d \propto (L/F)^{1-1/\alpha}, \tag{1}$$

where $\alpha = kT/E_0$ is the parameter already introduced in the introduction, L is the sample length and F the applied field. In the TOF experiment, the drift mobility μ_d is calculated from the measured transit time t_T of the carriers generated by the light pulse according to $\mu_d = L/t_T F$. To confront this method of determining the width of the distribution, E_0, with the one above, we have measured the temperature and field dependence of the hole drift mobility in a 27 μm thick a-Se cell. These results are shown in the traditional $\log(\mu_d)$ versus $10^3/T$ diagram in figure 4(a). Based on those results, the $\log(\mu_d)$ versus $\log(L/F)$ diagram of figure 4(b) is constructed that allows the determination of $\alpha(T)$ from the slopes $(1 - 1/\alpha)$. The temperature dependence of this parameter α is shown by the full symbols in figure 4(c). Although the values do not agree too well with the MT prediction for an exponential DOS, $\alpha = kT/E_0$, a 'best approximating' exponential with $E_0 \approx 22$ meV—indicated by the dashed line—can be obtained. Figure 4(c) also includes a second data set (open symbols) that was generated in similar fashion from the drift mobility data published by Kasap and Juhasz [29]. Here the agreement with the exponential DOS is better, giving 24 meV as the E_0 value.

In principle, a similar determination of the slope of the conduction band tail states can be envisioned since holes and electrons can be studied separately in the TOF experiment. However, as already found in [29] and as confirmed by the measurements shown in figure 5, the electron drift mobility in a-Se is independent of the applied electric field and equation (1) cannot be used. In fact, the field independence signifies that equilibrium carrier transport has been established before the transit time t_T of the electrons. Observation of such equilibrium transport rules out an exponential distribution of tail states on the conduction band side of the gap [30]. A Gaussian, or similar steeply decreasing DOS is needed to account for the experimental results.

While knowledge about the tail states can be deduced from the TOF transit time, later parts of the current transient contain information about the gap states. Free carriers are photo-excited at one contact of the sandwich cell and generate a transient current while drifting to the other electrode under the influence of an applied electric field. Carriers get trapped repeatedly in the process. At times larger than the transit time of the average carrier, t_T, the photocurrent is increasingly generated by the re-emission of carriers from deep traps. For $t \gg t_T$, the depth of the emitting trap can be approximated as $E_t = kT \ln(\nu t)$, where ν is an attempt-to-escape frequency of the order 10^{12} s^{-1}. The post-transit photocurrent $I(t)$ will then be proportional to the number of carriers released at time t from the density of states $g(E_t)$ at the corresponding energy level. Assuming equal capture probability into all states, the post-transit current $I(t)$ is directly related to the density of gap states $g(E)$ through the relations [31]:

$$I(t)t = \frac{Q_0 t_0 \nu}{2g(0)} g(E), \qquad E = kT \ln(\nu t), \tag{2}$$

where Q_0 is the total charge participating in the transient photocurrent, t_0 is the free-carrier transit time, and $g(0)$ is the DOS at mobility edge.

An example of electron TOF signals that include the post-transit part of the current transient is seen in figure 6(a). They were obtained at room temperature with a 2 μm thick sandwich

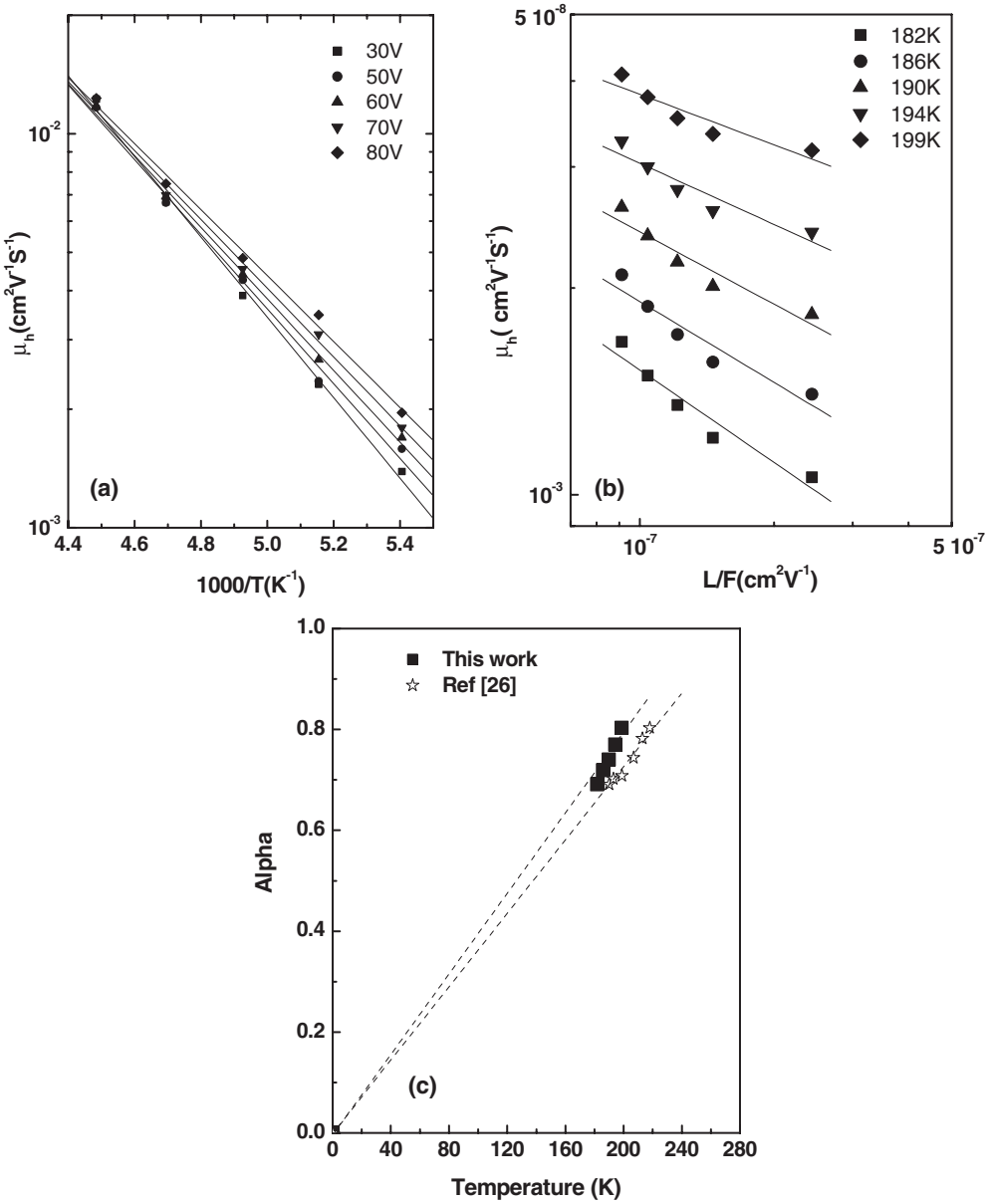

Figure 4. (a) Hole drift mobility data set from a 27 μm thick sandwich cell with Al bottom and Au top contacts; (b) drift mobility values taken from the fitted lines of part (a), plotted as a function of L/F for comparison with equation (1); (c) full squares: temperature dependence of the parameter α from equation (1) as calculated from the lines in part (b); open symbols: analogous results based on the data from [26].

with Al contacts, and with full intensity of the exciting light pulse. The latter no longer allows a correct measurement of the transit time, but raises the level of the post-transit current. Using the above equation (2), the post-transit current reveals an increased density of gap states centred some 0.53 eV below the conduction band edge, as illustrated in figure 6(b). This defect band

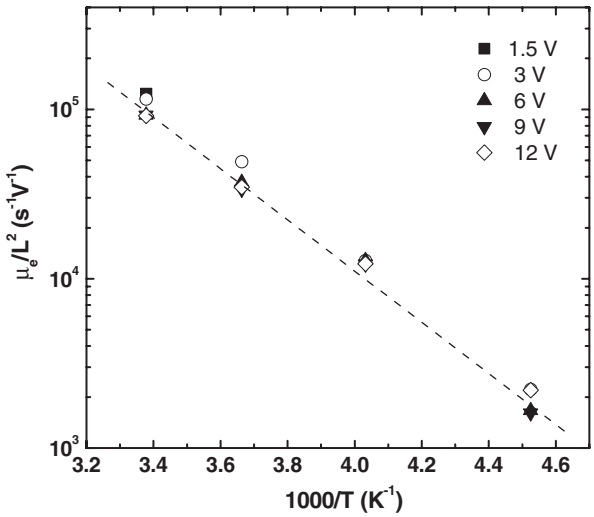

Figure 5. Electron drift mobility in a-Se as a function of inverse temperature and applied voltage. The dashed line corresponds to a 0.30 eV activation energy.

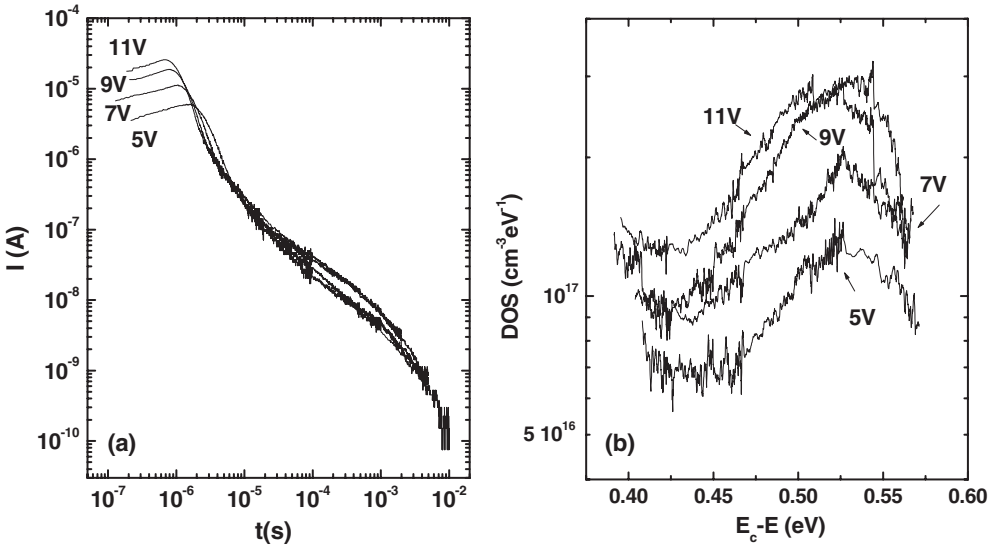

Figure 6. (a) Room-temperature TOF electron transients at four applied voltages across a 2 μm sample, under high illumination intensity to emphasize the post-transit part of the currents; (b) DOS below the conduction band tail, calculated with equation (2) for $t > 2t_T$ from the currents of (a) and with the parameters $L = 2$ μm, $T = 295$ K, $\mu_0 = 1$ cm^2 V^{-1} s^{-1}, $\nu = 10^{12}$ s^{-1}, $g(0) = 5 \times 10^{21}$ cm^{-3} eV^{-1} and $Q_0 = 6 \times 10^{-11}$ C (value for the 11 V curve).

was already reported in [17] and was identified with the occupied D^+ centre, $(D^+)^0$, from where electrons are re-emitted into the transport path. Analogous results were obtained with the TOF transients for holes shown in figure 7. They position a $(D^-)^0$ level ∼0.43 eV above the valence band. It should be noted at this point that the observation of the $(D^+)^0$ and $(D^-)^0$ levels in the post-transit currents is not automatically assured for all a-Se films. It was already pointed out

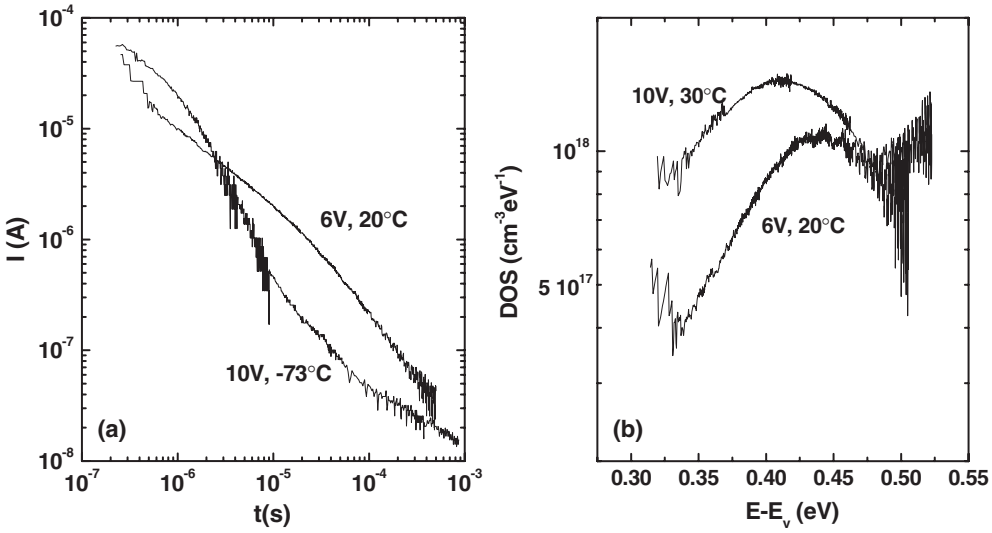

Figure 7. (a) Examples of hole current transients under indicated conditions and full light intensity. Only the low-temperature trace can show the carrier transit for the thin sample. (b) Defect band above the valence band tail as resolved from the 20 °C curve of part (a) and with the parameters $L = 1\ \mu$m, $T = 293$ K, $\mu_0 = 1\ \mathrm{cm^2\ V^{-1}\ s^{-1}}$, $\nu = 10^{12}\ \mathrm{s^{-1}}$, $g(0) = 5 \times 10^{21}\ \mathrm{cm^{-3}\ eV^{-1}}$ and $Q_0 = 1.3 \times 10^{-10}$ C, and an analogous transient measured at 30 °C.

in [32] that they can remain undetected against the background DOS of the tail and, possibly, other defect states. Nevertheless, the defect bands shown in figures 6(b) and 7(b) are detected in the majority of the samples, and always at their same respective energies. A careful study of the preparation conditions and pre-history of the various samples may be required to discover the reason behind the occasional failure to resolve the defect band.

4. Discussion

Surveying the experimental results from the preceding section, we recognize that the pattern that emerges for a-Se mirrors the one that is familiar from studies of the density of states of a-As_2Se_3. Discrete energy levels that can be linked to the negative-U centres are resolved from SSPC and the TOF post-transit currents, and a distribution of more or less exponentially distributed valence band tail states is indicated by the transient experiments. The positions in the band gap of the negative-U energy levels determined above are sketched in figure 8 with respect to a Fermi level position of E_F–$E_V = 0.95$ eV and a band gap of E_C–$E_V = 1.95$ eV at room temperature [33]. In figure 8, we use the notations T, A, O introduced by Elliott [22], to designate thermal, optical absorption, and other optical transitions levels. Within the experimental uncertainties, good agreement is found between the positions obtained for the thermally accessible levels of the defects, T^+ and T^-, from either SSPC or TOF measurements. The absorption band around 1.45–1.50 eV that is observed in the spectral response curves of figure 2, is most likely caused by transitions from the valence band to the A^+ level. The alternative of A^- to conduction band transitions is not feasible since the A^- level has to lie below the T^- level, which makes the distance to the band larger than 1.50 eV. The remaining transition level of the D^+ centre, i.e. the O^+ level, can be placed ∼0.8 eV above E_V on the basis of available photoluminescence data [10]. The small energy distance between the A^+

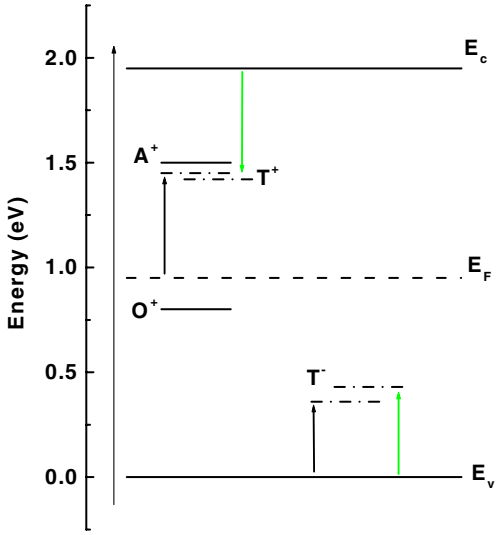

Figure 8. Sketch of the energy level diagram deduced for the negative-U coordination defects on the basis of the present study.

(This figure is in colour only in the electronic version)

and T^+ levels suggests that the D^+ defect has a rather flat energy profile in configuration space, in other words, that the energy increase due to the presence of an electron in the anti-bonding orbital [21] is roughly compensated by the polaronic lattice deformation energy. The larger energy distance between the O^+ level and the others indicates that the potential energy surface of the valence band has a stronger configurational dependence.

For the valence band tail states, the TOF drift mobility analysis predicts a much steeper exponential distribution than the one observed for a-As_2Se_3: a width of less than 25 meV for a-Se compared to the a-As_2Se_3 47 meV. The suggestion that our transient photodecay measurements failed to provide useful information because they did not meet the $T < T_0$ criterion that would have made the simple MT analysis applicable thus finds support in these low E_0 values. Complementary information on the a-Se conduction band tail states cannot be procured easily through photocurrent measurements: classical phototransients will only reflect the properties of the dominant carrier, which is the hole for the chalcogenides, and the TOF transients for electrons exhibit equilibrium characteristics, which necessitates a detailed fitting of the current transients with a complex set of analytical equations to extract an estimate for the DOS [18, 30].

There are relatively few previous literature results available to compare our analysis of the a-Se DOS with. Papers reporting initial work on a-Se from our laboratory [17, 24] do agree with the present more extensive and more closely controlled study. Similar to the drift mobility data set of figure 4, and the analogous one by Kasap and Juhasz that were used above, a further set by Marshall and Owen [34] is available. There the analysis leads to a 50% higher value, with E_0 of the order of 35 meV, but it should be noted that hot-pressed bulk a-Se samples were used rather than evaporated layers. For the conduction band side of the gap where the field independence of the mobility precluded the application of equation (1) to estimate the distribution of tail states, Koughia *et al* [18] used the TOF current transients themselves as input to a numerical model for the DOS. Although the authors focus on small-scale variations in the DOS, it is striking that the overall pattern does not deviate too much from an exponential

tail with $E_0 \approx 27$ meV. Since the same parts of the TOF transients are used that determine the transit times, and hence the field-independent drift mobilities, this 27 meV exponential cannot represent the true DOS near the conduction band, but it does suggest that the width of the valence and conduction band tails are comparable. The fact that both band tails are relatively narrow reduces the probability that the observation of the defect states is hindered by a background density due to those tails, as has been suggested for the case of a-As_2Se_3 [1]. In other words, our occasional failure to resolve those defects through TOF post-transit analysis should not be ascribed to a high tail-state density.

There are also some studies of the a-Se DOS that have come to conclusions which differ from ours. Orlowski and Abkowitz [19] concluded from a change of slope observed in transient photocurrents in the nanosecond range that there must be a prominent defect band some 0.25 eV above the valence band edge. To measure at those short times, they used a microstrip transmission line system with the a-Se as the dielectric. In our gap-cell geometry we cannot reach equally short times, but we should see the same break in the current traces at longer times when measuring at lower temperatures if indeed that defect band was present. We did not observe it in our samples. Abkowitz [20] found further support for the 0.25 eV level, as well as for a further defect at 0.35 eV below the conduction band edge, in the TOF measurements of Kasap and Juhasz, but, as outlined in [24], those values are based on a (historically determined) misinterpretation of the TOF data. The drift mobility data point in fact to a smooth, continuous distribution of states around those energies. Another feature of the a-Se DOS reported in [20] is the presence of defect bands near the middle of the band gap. Such mid-gap defects were used to model an anomalous dark current behaviour in [35], but the experimental reach of the present study is insufficient to allow us to explore the mid-gap region.

5. Conclusions

Photoconductivity measurements confirm the presence in amorphous selenium of two defect centres that show the characteristic properties of the negative-U co-ordination defects. The thermally accessible levels of these defects, T^+ and T^-, are located at 1.43 ± 0.02 eV and 0.40 ± 0.02 eV, respectively above the valence band mobility edge. These values, together with the optical transition energies of $\sim$1.50 eV for absorption and $\sim$0.80 eV for luminescence at the D^+ centre, are in line with corresponding values for the arsenic chalcogenides [6, 16] and show that the use of a-Se as a negative-U prototype is indeed justified.

On the other hand, less similarity is found for the tail-state distributions between a-Se and the other chalcogenides. Whereas the wide exponential valence band tail of a-As_2Se_3 has become emblematic for the group, a-Se has much steeper and not strictly exponential band tails. The 'exponential width' $E_0 \approx 24$ meV deduced in this paper will need further refinement through low-temperature measurements of the transient photocurrents.

Acknowledgments

We thank Professor Kasap for providing us with some thick, excellent a-Se layers. One of us (MLB) thanks the Belgian Technical Cooperation agency for a PhD grant. Financial support for this research by the *Fonds voor Wetenschappelijk Onderzoek—Vlaanderen* is gratefully acknowledged.

References

[1] Adriaenssens G J and Qamhieh N 2003 *J. Mater. Sci. Mater. Electron.* **14** 605
[2] Anderson P W 1975 *Phys. Rev. Lett.* **34** 953

[3] Street R A and Mott N F 1975 *Phys. Rev. Lett.* **35** 1293
[4] Agarwal S C 1973 *Phys. Rev.* B **7** 685
[5] Tanaka Ke 2001 *J. Optoelectron. Adv. Mater.* **3** 189
[6] Street R A 1976 *Electronic Phenomena in Non-Crystalline Semiconductors* ed B T Kolomiets (Leningrad: Nauka) p 116
[7] Mott N F, Davis E A and Street R A 1975 *Phil. Mag.* **32** 961
[8] Vardeny Z and Tauc J 1985 *Phys. Rev. Lett.* **54** 1844
[9] Main C and Owen A E 1973 *Electronic and Structural Properties of Amorphous Semiconductors* ed P G Le Comber and J Mort (London: Academic) p 527
[10] Street R A, Searle T M and Austin I G 1974 *Phil. Mag.* **29** 1157
[11] Depinna S P, Cavenett B C and Lamb W E 1983 *Phil. Mag.* B **47** 99
[12] Mott N F and Davis E A 1979 *Electronic Processes in Non-Crystalline Materials* 2nd edn (Oxford: Clarendon)
[13] Schmidlin F W 1977 *Phys. Rev.* B **16** 2362
[14] Orenstein J and Kastner M 1981 *Phys. Rev. Lett.* **46** 1421
[15] Monroe D and Kastner M A 1986 *Phys. Rev.* B **33** 8881
[16] Adriaenssens G J 1990 *Phil. Mag.* B **62** 79
[17] Song H Z, Adriaenssens G J, Emelianova E V and Arkhipov V I 1999 *Phys. Rev.* B **59** 10607
[18] Koughia K V, Fogal B, Belev G, Johanson R E and Kasap S O 2004 *J. Non-Cryst. Solids* **338** 569
[19] Orlowski T E and Abkowitz M 1985 *J. Non-Cryst. Solids* **77** 439
[20] Abkowitz M 1988 *Phil. Mag. Lett.* **58** 53
[21] Kastner M, Adler D and Fritzsche H 1976 *Phys. Rev. Lett.* **37** 1504
[22] Elliott S R 1990 *Physics of Amorphous Materials* 2nd edn (Harlow: Longman)
[23] Popescu M A 2000 *Non-Crystalline Chalcogenides* (Dordrecht: Kluwer)
[24] Qamhieh N, Benkhedir M L, Brinza M, Willekens J and Adriaenssens G J 2004 *J. Phys.: Condens. Matter* **16** 3827
[25] Vanderbilt D and Joannopoulos J D 1982 *Phys. Rev. Lett.* **49** 823
[26] Simmons J G and Taylor G W 1974 *J. Phys. C: Solid State Phys.* **7** 3051
Simmons J G and Taylor G W 1974 *J. Phys. C: Solid State Phys.* **7** 3067
[27] Moustakas T D and Weiser K 1975 *Phys. Rev.* B **12** 2448
[28] Okamoto H, Kida H and Hamakawa Y 1984 *Phil. Mag.* B **49** 231
[29] Kasap S O and Juhasz C 1985 *J. Phys. D: Appl. Phys.* **18** 703
[30] Brinza M, Emelianova E V, Stesmans A and Adriaenssens G J 2004 *Mater. Res. Soc. Symp. Proc.* **808** A5.6
[31] Seynhaeve G F, Barclay R P, Adriaenssens G J and Marshall J M 1989 *Phys. Rev.* B **39** 10196
[32] Emelianova E V, Qamhieh N, Brinza M, Adriaenssens G J, Kasap S O, Johanson R E and Arkhipov V I 2003 *J. Non-Cryst. Solids* **326** 215
[33] Tichy L, Ticha H, Nagels P, Sleeckx E and Callaerts R 1996 *Mater. Lett.* **26** 279
[34] Marshall J M and Owen A E 1972 *Phys. Status Solidi* a **12** 181
[35] Qamhieh N, Willekens J, Brinza M and Adriaenssens G J 2003 *J. Phys.: Condens. Matter* **15** L631